Composition of Grain Boundaries and Interfaces: A Comparison of Modern Analytical Techniques using a 300 kV FEGTEM

V J Keast, P A Midgley, S J Lloyd, P J Thomas, M Weyland, C B Boothroyd and C J Humphreys

Department of Materials Science and Metallurgy, University of Cambridge, Pembroke Street, Cambridge, CB2 3QZ.

ABSTRACT: Interfacial reactions and grain boundary segregation are often the limiting factors to the performance of functional and structural materials so the need for quantitative compositional information at the nanometre level is as great now as ever. The advent of new field emission TEMs has seen the emergence of new techniques for such high spatial resolution microanalysis. In this paper we will consider the relative merits of (STEM-based) X-ray mapping and HAADF imaging and (TEM-based) EFTEM and Fresnel imaging. All these techniques can now be performed on a single instrument and on the same area and thus, in principle, direct comparisons can be made with confidence.

1.   INTRODUCTION

In recent years the arrival of commercial (S)TEMs with stable field emission guns has led to remarkable progress in the microanalysis of boundaries and interfaces. This has been particularly evident in the analysis of semiconductor systems using STEM-based techniques combining HAADF imaging (to reveal atomic number or 'Z' contrast) and energy loss spectroscopy (e.g. Muller et al 1999). On the other hand, fast compositional mapping over large areas using TEM-based techniques is becoming more quantitative and reliable (Thomas et al 1999). With the variety of microanalytical techniques now available for compositional analysis, including EFTEM and EELS, HAADF imaging, X-ray mapping, Fresnel imaging and electron holography, it is perhaps timely to review some of these techniques and comment upon their relative merits. At Cambridge we have started such an assessment using a Philips CM300 FEGTEM and in this paper we show recent results from three 'test cases' that highlight the advantages of each technique and discuss some of the problems and artefacts that can occur during analysis.

2.   EXPERIMENTAL METHODS

The Schottky field emitter, as used on the Philips CM300 FEGTEM, is fast becoming the preferred choice for a FEG because of the combination of high brightness and large total current. By demagnifying the source, very small, coherent probes can be formed which make it extremely suitable for near-atomic scale analysis. As an example, Fig. 1 shows a ronchigram taken from the <110> zone axis of Si together with its Fourier transform. In contrast, for EFTEM and related techniques, where signal to noise considerations can be paramount, the Schottky source is able to yield a total current of 300 nA at the specimen (Botton and Phaneuf 1999).
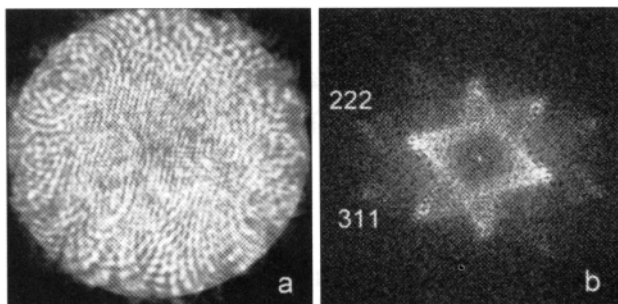
Fig. 1 (a) A ronchigram and (b) its Fourier transform taken from the <110> zone axis of Si. The {222} and {311} 'reflections' in the transform indicate a coherent probe width of ~1.5Å in diameter.

In addition to a standard X-ray detector and Gatan imaging filter, the instrument in Cambridge is equipped with an on-axis Fischione-designed HAADF detector which sits just above the viewing chamber. The ratio of the inner to outer radius is fixed at 1:6 but by simply adjusting the camera length it is possible to vary the inner radius from 1 mrad to 100 mrad and larger radii are achievable if required. The ability to adjust the inner radius is crucial if truly incoherent conditions are required for HAADF imaging as will be discussed later.

3.   RESULTS

3.1 Grain Boundary in Oxidised FeCrAl Alloy.

The first example is that of a grain boundary in an oxide dispersion strengthened (ODS) FeCrAl alloy which has undergone oxidation so as to form an alumina scale. Fig. 2(a) shows a bright field (zero-loss) image and (b) a Ti elemental map taken from a grain boundary which shows segregation of Ti to the boundary. The Ti map was acquired using a large series of EFTEM images and analysed by 'image spectroscopy', about which more details can be found in these proceedings (Thomas et al 1999). No other segregants were found were detected at the boundary and from previous studies (Newcomb 1997), such boundaries are known to be amorphous. Quantitative analysis of the map gave a maximum Ti composition of ≈5 at.% and a boundary width of 2.8nm (FWHM), as seen in the insert of Fig. 2(b).
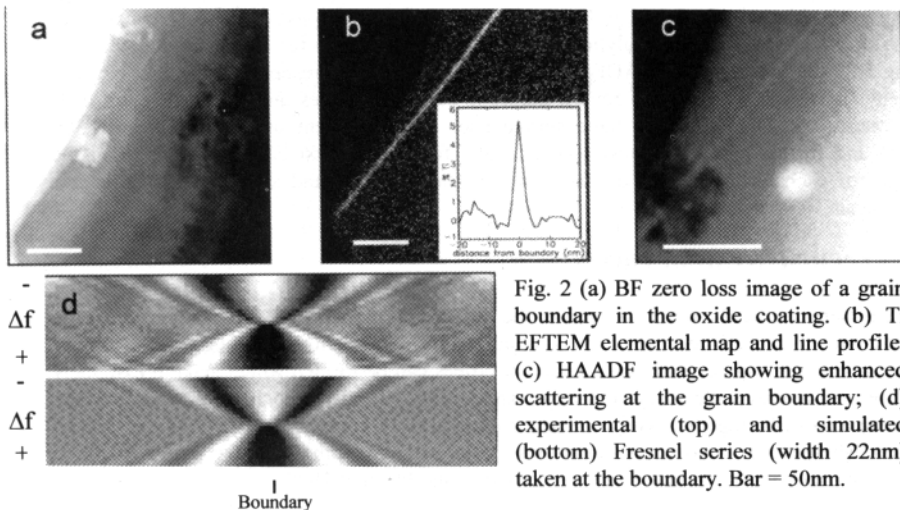

Fig. 2 (a) BF zero loss image of a grain boundary in the oxide coating. (b) Ti EFTEM elemental map and line profile; (c) HAADF image showing enhanced scattering at the grain boundary; (d) experimental (top) and simulated (bottom) Fresnel series (width 22nm) taken at the boundary. Bar = 50nm.

Fig. 2(c) shows a HAADF image taken under incoherent conditions so that the image showed Z-contrast (see next section) and confirms the presence of a strong scatterer at the Ti-doped boundary. Assuming a Z^2 dependence the peak Ti content was determined to be 9 at.%.

Fresnel imaging is very sensitive to changes in the mean inner potential and thus, amongst other things, to changes in the atomic number density. An experimental Fresnel series was matched by simulation as shown in Fig. 2(d). This yielded a real part of the boundary potential well that was 1.3V deep and 1.3nm wide (half that given by EFTEM). The imaginary part of the potential was positive indicating strong absorption (i.e. strong high angle scattering) and the presence of a heavy element. The reduction in potential at the boundary is consistent with its amorphous nature (lower density) and the addition of Ti (presumably as the oxide) is not sufficient to push it positive. Using the boundary width given by the Fresnel analysis raises the peak composition determined by EFTEM to $\approx 10\%$ in good agreement with the HAADF imaging. Substituting 10% TiO_2 into crystalline alumina leads to a potential 'hill' of $\approx 2V$ and thus to measure a potential well of 1.3V at the boundary would require a volume decrease in the amorphous phase of $\approx 15\%$ compared with the surrounding crystalline matrix.

3.2 Precipitation at a Grain Boundary in Annealed 316 Stainless Steel

In this study we again compare EFTEM and HAADF images. Fig. 3(a) shows a BF zero-loss image of carbide precipitates at the boundary of an annealed 316 stainless steel. Figs 3(b) and (c) show elemental maps indicating Cr and Mo rich precipitates, respectively. Figs 3(d) and (e) show HAADF images taken from the same area at two different camera lengths. Fig. 3(d) has been taken with an inner radius that corresponds to 20mrad , whereas in Fig. 3(e) the inner radius was 80 mrad. It is clear from the appearance of dislocations and a change in contrast at the boundary that the image in Fig. 3 (d) contains phase contrast, i.e. the scattering is partially coherent. The intensity of such an image will certainly not be proportional to Z^2! Therefore, it is vital that the conditions needed for truly incoherent images are known if correct statements are to be made pertaining to 'Z-contrast'. The precipitates seen in the Z-contrast image of Fig. 3(e) are Mo-rich, c.f. Fig. 3(c). The bright band surrounding the grain boundary in the same figure and the dark region surrounding the precipitates is due to substantial changes in thickness verified using independent measurements.
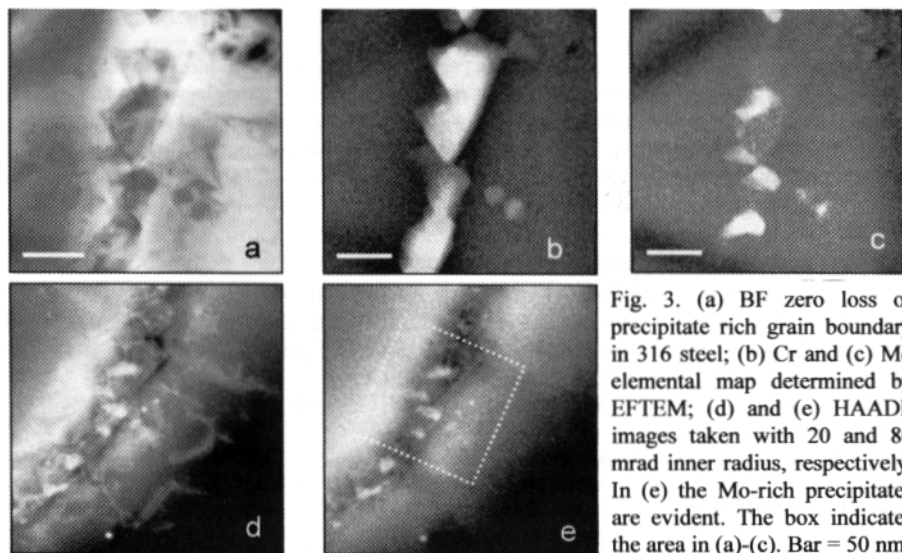

Fig. 3. (a) BF zero loss of precipitate rich grain boundary in 316 steel; (b) Cr and (c) Mo elemental map determined by EFTEM; (d) and (e) HAADF images taken with 20 and 80 mrad inner radius, respectively. In (e) the Mo-rich precipitates are evident. The box indicates the area in (a)-(c). Bar = 50 nm.

3.3 Ag-Ni Multilayers

In the last study we contrast the ability of EFTEM, HAADF imaging and X-ray mapping to yield high resolution information regarding the composition of a 4.3nm period magnetron-sputtered Ag-Ni multilayer structure (Schweitz et al 1999). Figs 4(a) and (b) show X-ray Ag and

Ni maps, respectively, taken on a VG HB501 STEM. Fig. 4(c) is a HAADF image taken under incoherent conditions which clearly shows the Ag layer. Figs 4 (d) and (e) are Ag and Ni EFTEM elemental maps, respectively. Line profiles taken from the maps indicated the EFTEM maps had the best spatial resolution. The spatial resolution of STEM-based mapping using X-rays or HAADF images will be limited by beam broadening effects and this can be significant for relatively thick samples such as those prepared using the FIB, including this one where the thickness, $t \approx 80nm$.
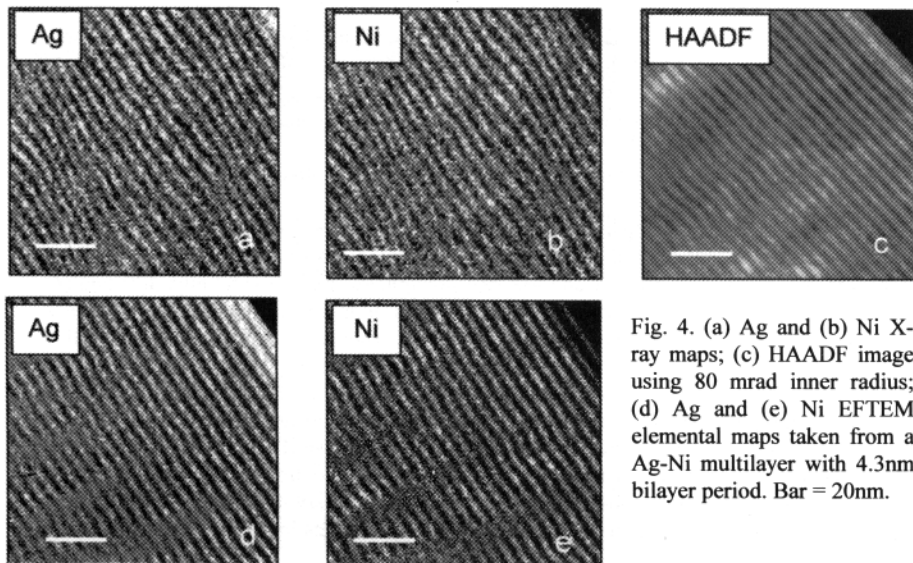

Fig. 4. (a) Ag and (b) Ni X-ray maps; (c) HAADF image using 80 mrad inner radius; (d) Ag and (e) Ni EFTEM elemental maps taken from a Ag-Ni multilayer with 4.3nm bilayer period. Bar = 20nm.

4.   CONCLUSIONS

On modern FEGTEM instruments there are a variety of techniques available for microanalysis. This paper has shown that many of these techniques are complementary and can often support or add information rather than simply duplicate. Results presented here illustrate that if care is taken to avoid artefacts then by using more than one technique the characterisation of interfaces and boundaries will become more complete.

REFERENCES

Botton G and Phaneuf M W 1999 *Micron* **30** 109

Krivanek O L, Kundman M K and Kimoto K 1995 *J Microscopy* **180** 277

Muller D A, Sorsch T, Moccio F H, Baumann K, Evans-Lutterodt K. and Timp G 1999 *Microsc. Microanal.* **5** (Suppl 2: Proceedings) (New York:Springer-Verlag) p190-191

Newcomb S B 1997 *Inst Phys Conf Series* **153** 289 (Bristol:IOPP)

Schweitz K O, Ratzke K, Foord D T, Greer A L, Thomas P J, Geisler H, Chevallier J and Bottiger J 1999 (submitted to *Phil. Mag A*)

Thomas P J, Midgley P A and Spellward P 1999 (these proceedings)

ACKNOWLEDGEMENTS